Hindawi
Advances in Civil Engineering
Volume 2022, Article ID 4068995, 7 pages
https://doi.org/10.1155/2022/4068995

Research Article

Dynamic Response Analysis of Super Shallow-Buried Rectangular Tunnel

Sanqing Su[1], **Tao Yin**[1], **Zhen Cao**[1], **Bin Lei**[1], **Zhao Liu**[2], **Wenxu Lin**[3] and **Anyuan Kuang**[4]

[1]*School of Civil Engineering, Xi'an University of Architecture and Technology, Xi'an, Shaanxi 710055, China*
[2]*Ankang Highway Administration of Shaanxi Province, Ankang 725000, Shaanxi, China*
[3]*Municipal Civil Air Defense Office, Ankang Housing and Urban-Rural Development Bureau, Ankang 725000, Shaanxi, China*
[4]*Shaanxi Construction Engineering Twelfth Construction Group Co Ltd., Ankang 725000, China*

Correspondence should be addressed to Zhen Cao; railcaozhen@xauat.edu.cn and Bin Lei; leibin@xauat.edu.cn

Received 18 January 2022; Accepted 16 April 2022; Published 9 June 2022

Academic Editor: Marco Filippo Ferrotto

Relying on the project of the open-cut municipal tunnel undercrossing Ankang Freight V yard, the train dynamic response and seismic response of ultrashallow-buried rectangular tunnel of the lower interchange are studied, respectively, by combining the method of field measurement and numerical simulation. The results show that under the action of train vibration load, the dynamic stress response of the top plate midspan and the upper end of the side wall of the tunnel cross section directly below the rail is the most significant, and the dynamic stress response of the bottom plate is the smallest. Under the rare earthquake, the tunnel structure has large transverse deformation, in which the transverse displacement of the tunnel roof is the largest. At the same time, there is a large stress concentration at the variable section of the tunnel.

1. Introduction

With the development of cities, the demand for the construction of transportation facilities is increasing, and the situation where the newly built line intersects with the already-built line is also gradually increasing. Due to the limitations of existing lines and the need for comprehensive development and utilization of underground space, a large number of undercrossing tunnels have appeared, and especially, there are many engineering examples of new tunnels built in close distance under the existing railway line. The existing design methods simplify the train load into medium load without considering the influence of dynamic stress caused by train operation [1]. This static design idea often underestimates the effect of the upper train's dynamic stress. For example, the investigation of the undercrossing tunnels of the management section of the Hangzhou Railway branch of the China Railway Administration showed that there were 5 different undercrossing tunnels cracking within a range of more than 60 kilometers from K12 + 500 to K75 + 600, and the maximum crack width was up to 1 mm. Therefore, this kind of problem has become an important and unavoidable problem in the current underground structure design. At present, the research on undercrossing tunnel mainly focuses on the impact of proximity construction of tunnel undercrossing existing railway lines [2–9] and the dynamic response of the tunnel structure. For example, Chai [10] took a tunnel passing through the Beijing-Shanghai high-speed railway as the research background and used FLAC3D software to simulate the dynamic response law of the underlying tunnel lining structure under the action of train vibration loads and different construction stages. Zheng et al. [11] obtained the longitudinal distribution law of tunnel vault pressure under dynamic train load by using three-dimensional calculation. In addition, a large number of earthquake disasters indicate that the underground structure, such as the metro tunnel, is not safe and reliable as people think and can also be destroyed and

Figure 1: Schematic diagram of the tunnel undercrossing the existing railway line.

Figure 2: Positional relationship between horizontal steel bars in tunnel cross section and existing railway line.

collapsed under the action of an earthquake [12, 13]. Therefore, the research on the seismic response of underground structures can also not be ignored. For example, Wang et al. [14] used 3D nonlinear finite element software to study the seismic response of the cross-sectional tunnel of Hangzhou Metro Line 1 and provided the calculation results of the seismic response of the subway tunnel and the variation law of lining deformation stress. Some scholars start from the dynamic interaction of soil-underground structure and conduct seismic research and analysis of underground structure by using experimental research and numerical simulation methods [15, 16]. Throughout the research literature on the underground structure, there is a lack of research on the dynamic response of ultrashallow-buried tunnel structure at the lower interchange during train operation, and extreme cases such as the seismic response of ultrashallow-buried tunnels are even less considered. Therefore, by studying the dynamic response of ultrashallow-buried tunnel structure under train vibration and earthquake, respectively, it provides a theoretical basis for the structural design and safe operation of ultrashallow-buried tunnel at the lower interchange, which has important theoretical significance in and engineering practical value.

2. Project Overview

This topic originates from the construction project of the Jiangbei section of the main road around the city in Ankang City, China (hereinafter, referred to as the north ring line). The starting section of the north ring line passes through the existing Ankang East freight station in the form of a tunnel, in which the proposed tunnel is of left and right split type,

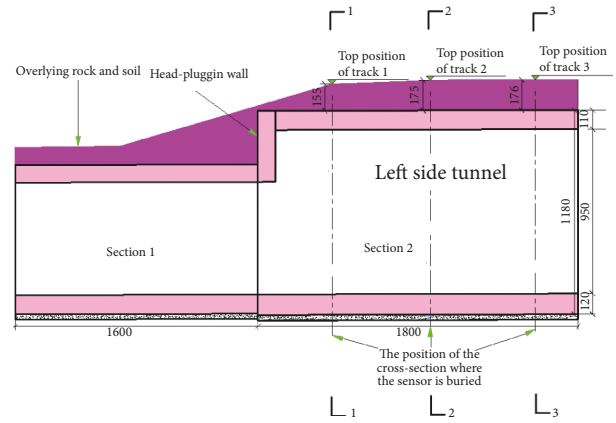

Figure 3: Schematic diagram of the cross section where the sensor is located (unit: cm).

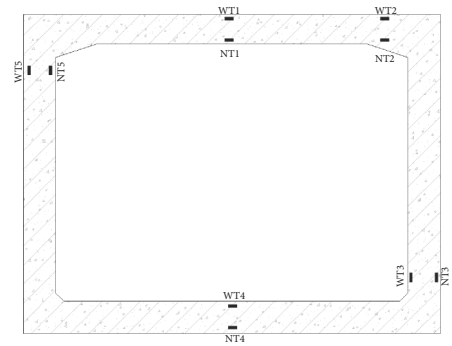

Figure 4: Layout diagram of concrete stress gauges of 1-1 profile ~3-3 profile.

with a net distance of 7.2 m between the two tunnels. The tunnel crosses 13 tracks of Ankang East freight station from south to north, with a total length of 170 m, as shown in Figure 1. The cross section of the tunnel is rectangular, and the lower part of the tunnel bottom plate is a 30 cm thick C20 concrete cushion, and the average thickness of the covering soil on the roof of the tunnel is 1.5 m. The tunnel is a concrete structure with a concrete strength grade of C40, in which the horizontal steel bars in the tunnel cross section are parallel to the railway line, as shown in Figure 2. In addition, geological survey results show that the soil of the site from top to bottom is the Quaternary Holocene artificial accumulation layer Q_4^{ml} plain fill, the Quaternary Holocene alluvial layer silty clay, the Quaternary upper alluvial layer Q_3^{al}(silty clay), and pebble soil.

3. Field Monitoring and Analysis

3.1. Sensor Installation Scheme. Additional dynamic stress will be generated inside the underlying tunnel structure under the action of the train vibration load. In order to directly reflect the dynamic stress response law of each part of the tunnel under the action of the train dynamic load, the second section tunnel is selected as the monitoring object, and concrete stress gauges are arranged in the tunnel cross sections directly below the 1~3 tracks, respectively, as shown

Figure 5: Installation diagram of a group of concrete stress gauges.

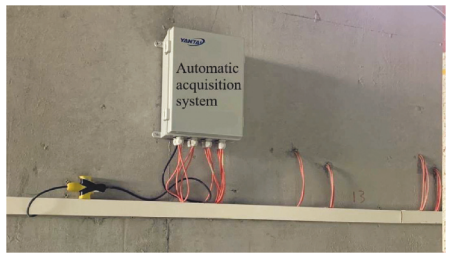

Figure 6: Schematic diagram of the automated acquisition system.

in Figure 3. It can be seen from Figure 3 that there is no train track above the first section of the tunnel. The cross-section heights of the two sections of the tunnel are different, and their variable cross-section positions are connected by a head-plugging wall. Five groups of monitoring points are set up at each cross section in the second section of the tunnel, and the specific locations and corresponding numbers are shown in Figures 3 and 4. The field installation diagram of one group of concrete stress gauges is shown in Figure 5. In addition, the cross section of the tunnel has a span of 15 m and a height of 11.8 m, and the thickness of the side wall and bottom plate is 1.2 m; the thickness of the top plate is 1.1 m; the thickness of the head-plugging wall is 1 m.

After the sensor is installed, the sensor cable is led out and connected to the automatic acquisition box, as shown in Figure 6. After the tunnel is completed, when the train passes above the tunnel, the automatic acquisition system sends the data collected on-site to the platform through wireless communication technology, and after the data are analyzed and processed, the monitoring results are obtained.

3.2. Field Monitoring Results Analysis. During the operation period, the dynamic stress limit of tunnel structure refers to the "code for design on reinforced and prestressed concrete structure of railway bridge and culvert [17]," and the tensile and compressive dynamic stresses of concrete structures under repeated train loads are stipulated as follows:

$$\sigma_{ct} \leq 0.7 f_{ct}, \tag{1}$$

$$\sigma_{c} \leq 0.55 f_{c}, \tag{2}$$

where σ_{ct} is the tensile stress of concrete structure (MPa), f_{ct} is the ultimate tensile strength of concrete (MPa), σ_c is the compressive stress of concrete structure (MPa), and f_c is the ultimate compressive strength of concrete (MPa).

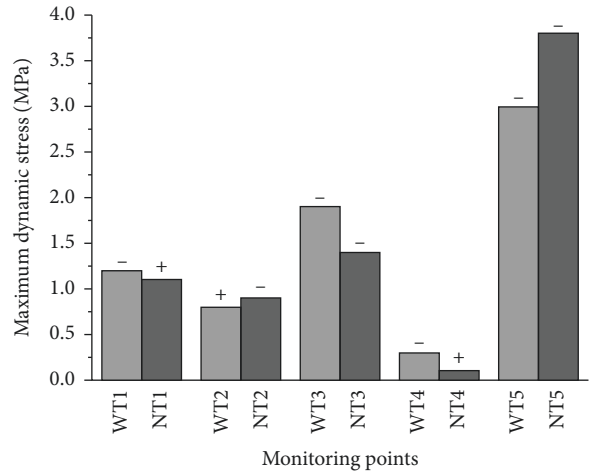

Figure 7: Maximum dynamic stress value of each monitoring point.

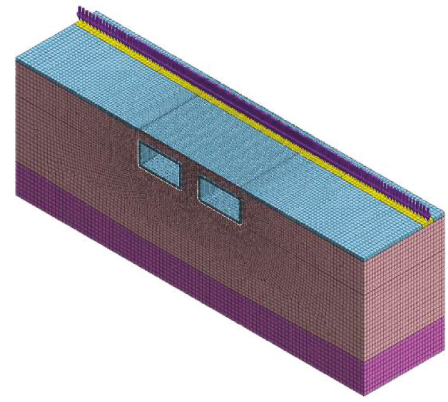

Figure 8: Schematic diagram of 3D finite element model.

Since the ultimate tensile strength of C40 concrete is 2.7 MPa and the ultimate compressive strength is 27 MPa, the tensile and compressive dynamic stress limits of the tunnel structure are 1.89 MPa and 14.85 MPa, respectively, according to the above formula.

According to the on-site monitoring results, when the trains with the same counterweight and the same speed pass through the three tracks above the tunnel, respectively, the dynamic stress generated by the tunnel cross section directly below each track is approximately the same. Therefore, the dynamic stress distribution of only one of the tunnel cross sections is studied. Among them, the model of the passing train is a P70 boxcar, about 40, each with a length of 16 m, a wheelbase of 1.83 m, an average weight of 70 t per boxcar, and a speed of 45 km/h. Under the above working conditions, the dynamic stress at each monitoring point of the tunnel cross section directly below the second track is shown in Figure 7 ("+" in the figure represents tensile stress, and "–" represents compressive stress). It can be seen from the figure that the maximum horizontal dynamic tensile stress occurs top plate midspan directly below the rail, and its value is

Table 1: Material physical and mechanical parameters table.

Material	Elastic modulus/Gpa	Poisson's ratio	Density/(kN·m^{-3})	Cohesion/kPa	Internal friction angle/(°)	Thickness (m)
Plain fill	0.006	0.3	18.5	8	10	2
Silty clay	0.012	0.3	19.6	32	15	22
Pebble layer	0.046	0.2	21.2	0.1	40	16

Table 2: Material physical and mechanical parameters table.

Structure name	Category	Elastic modulus/Gpa	Poisson's ratio	Density/(kN·m^{-3})
Ballast	Gravel ballast	0.01	0.3	18
Tunnel lining	C40 concrete	32.5	0.2	25

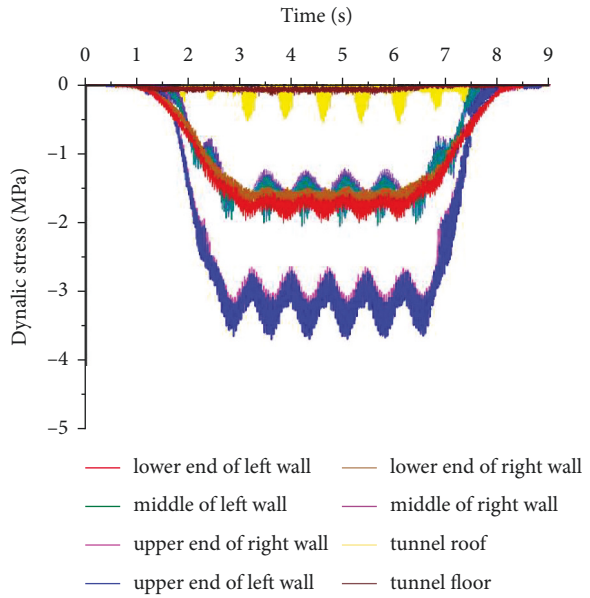

Figure 9: Time-history curve of dynamic compressive stress at each part of the left tunnel cross section.

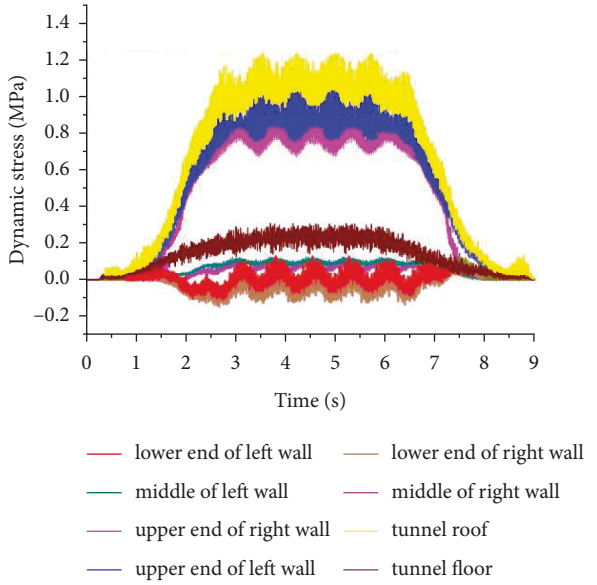

Figure 10: Time-history curve of dynamic tensile stress at each part of the left tunnel cross section.

1.1 MPa, which reaches 59% of the ultimate tensile strength of concrete. The maximum vertical dynamic compressive stress appears at the upper end of the side wall, and its value is 3.8 MPa, which reaches 26% of the ultimate compressive strength of concrete. It can be seen that the damage to the tunnel structure is mainly controlled by the tensile strength. From the stress vibration index, when the train passes over the tunnel, the tensile and compressive dynamic stresses of the structure are far less than the dynamic stress limit of the concrete material, which shows that a single train vibration load will not cause the strength damage of the tunnel structure. From the overall distribution of dynamic stress of the tunnel structure, the train vibration load has a relatively great impact on the upper end of the tunnel side wall and the top plate, and the dynamic stress of each monitoring point of the structure decreases with the increase of the distance from the vibration source. Among them, the dynamic stress of the tunnel bottom plate furthest from the vibration source decreases by 90% compared with the dynamic stress of the tunnel top plate, indicating that the dynamic stress response of the tunnel structure decays rapidly.

4. Numerical Simulation Analysis

4.1. Model Building. In addition to field monitoring, the corresponding finite element model is established with the help of midas GTS NX for numerical simulation. Considering the boundary effect, the size of the stratum model is length × width × height = 146 m × 34 m × 40 m, as shown in Figure 8. The stratum model adopts the hybrid grid dominated by hexahedron, and the tunnel model adopts a quadrilateral grid. The meshes closer to the tunnel are denser, and the meshes farther from the tunnel are coarser. The minimum unit size in the overall model is 50 cm, and the maximum unit size is 100 cm. In addition, roller horizontal constraints are applied to the periphery of the stratum model, and the vertical constraints are applied to the bottom. The static boundary is selected as the boundary condition of dynamic calculation, so as to suppress the reflection of vibration wave on the model boundary. Due to the fact that there are many freight train carriages in the actual situation, it is impossible to simulate all of them due to the limitation of calculation conditions. Therefore, targeted verification and analysis are required. In the numerical simulation

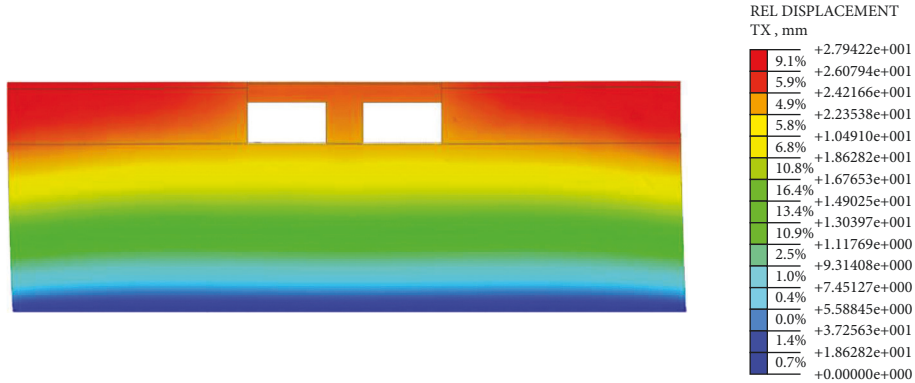

Figure 11: Transverse relative displacement of the stratum.

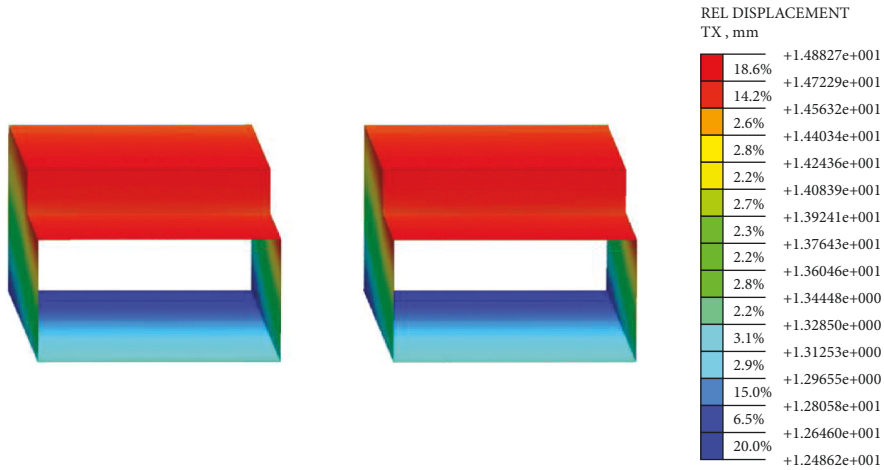

Figure 12: Tunnel transverse relative displacement.

working conditions, it is only considered that the train is six carriages and passes through the middle track above the tunnel. Other working conditions of simulated train dynamic load are the same as those of the actual train.

4.2. Material Constitutive Relationship and Calculation Parameters. The elastic-plastic model is selected for the surrounding rock, and the Mohr-Coulomb yield criterion was followed. According to the site geological survey data, the soil of the site is plain fill, silty clay, and pebble soil from top to bottom, and the physical and mechanical parameters of the formation are shown in Table 1. The elastic model is selected for the tunnel structure and ballast, and the corresponding parameters are shown in Table 2.

4.3. Model Verification. According to the numerical simulation results, under the action of train vibration load, the dynamic stress of the left and right line tunnels is symmetrically distributed. Among them, the dynamic stress time-history curve of each part of the left tunnel section is shown in Figures 9 and 10. It can be seen from the figure that the dynamic stress amplitude near the vibration source fluctuates greatly, and the dynamic stress amplitude far away from the vibration source fluctuates less. Secondly, the peak value of dynamic stress at each part of the tunnel cross section is different. Among them, the dynamic tensile stress at the top slab midspan is the largest, with the maximum peak value of 1.13 MPa, and the dynamic compressive stress at the upper end of the side wall is the largest, with the maximum peak value of 3.9 MPa. The dynamic stress at the bottom plate is the smallest, with the peak value of dynamic tensile stress of 0.3 MPa and the peak value of dynamic compressive stress of 0.2 MPa. The peak value of dynamic stress at each part calculated by numerical simulation is basically consistent with the measured value in Section 3.2, which shows that the numerical simulation can better restore the actual situation of the site. It also proves that the numerical model has good similarity and reliability, which can be used for further seismic analysis.

4.4. Seismic Response Analysis. A free field boundary is added on the basis of the verified three-dimensional numerical model, and then, a Taft seismic wave with a peak acceleration of 0.2 g is input for linear time history analysis. As shown in Figures 11 and 12, it can be seen from the cloud diagram of transverse relative displacement of the stratum and the tunnel that under the action of the rare earthquake, the transverse displacement of the whole stratum is inversely

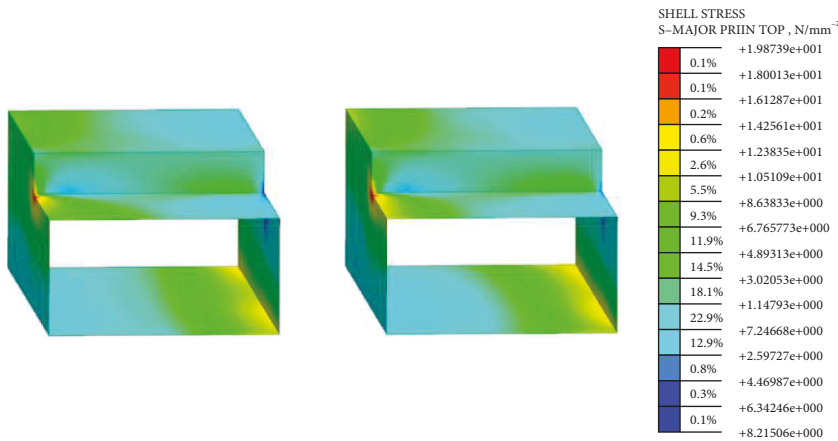

Figure 13: Principal stress cloud diagram of the tunnel.

proportional to the buried depth of the soil, in which the maximum transverse displacement occurs in the upper soil layer, which is 28 mm, indicating that shallow-buried tunnels are more susceptible to earthquake damage than deep-buried tunnels. This is consistent with Sharma and other scholars' investigation conclusions on seismic damage to underground structures [18–20]. Secondly, the maximum transverse displacement of the tunnel structure appears in the top plate of the tunnel, which is 15 m, and the minimum transverse displacement appears in the bottom plate of the tunnel, which is 12 mm, indicating that the tunnel has large transverse deformation. As shown in Figure 13, it can be seen from the tunnel stress cloud diagram that when the tunnel has large transverse deformation, there is a large stress concentration at the variable section of the tunnel, in which the principal tensile stress at the variable section on the left side of the tunnel reaches 20 MPa, the principal compressive stress at the variable section on the right side of the tunnel reaches 8 MPa, and the seismic response on the left side is more obvious than that on the right side. In addition, the tensile stress and compressive stress of the entire tunnel cross section are distributed diagonally symmetrical; that is, one pair of opposite corners and the periphery of the tunnel are under tension, and the other pair of opposite corners and the periphery are under compression.

5. Conclusion

In this paper, the train dynamic response and seismic response of lower interchange ultrashallow-buried tunnel structure are analyzed. The main conclusions are as follows:

(1) The dynamic stress amplitude of the tunnel structure decreases with the increase of the distance from the vibration source. Either in absolute value or upper and lower vibration amplitude, the dynamic tensile stress of the midspan of the tunnel roof and the dynamic compressive stress of the upper end of the side wall are obviously larger than those of other parts. The proportion of the maximum dynamic tensile stress in the ultimate tensile strength of concrete is significantly greater than that of the maximum dynamic compressive stress in the ultimate compressive strength of concrete. Therefore, the failure of the tunnel structure is mainly controlled by the tensile strength.

(2) Under the rare earthquake, the tunnel structure appears large transverse deformation, and the transverse displacement of the upper part of the tunnel is significantly greater than that of the lower part of the tunnel, in which the transverse displacement of the tunnel roof is the largest. There is a large stress concentration at the variable cross-section position of the tunnel, in which the maximum principal tensile stress appears at the variable cross-section position on the left side of the tunnel, with a value of 20 MPa, and the maximum principal compressive stress occurs at the variable cross-section position on the right side of the tunnel, with a value of 8 MPa. Therefore, in the actual project, the thickness of the head-plugging wall at the variable cross-section position can be appropriately increased, and the connection with the side wall can be strengthened to reduce the impact of earthquake action.

Data Availability

The data used to support the findings of this study are included within the article.

Conflicts of Interest

The authors declare that they have no conflicts of interest.

References

[1] The Third Survey and Design Institute of the Ministry of Railways, "General Code for Design on Railway Bridges and Culverts (TB10002.1-99)," China Railway Press, Beijing, China, 2000..

[2] J. Zheng, "Application of key construction technology for shield undercrossing railway station area," *Journal of Shijiazhuang Tie dao University*, vol. 31, no. 3, pp. 29–35, 2018.
[3] Y. L. Ding, "Key technology research on four parallel lines of metro underpassing railway track and station house," *Railway Construction Technology*, vol. 01, pp. 82–86, 2018.
[4] Y. J. Lu, "Analysis and measures for risk of metro shield tunneling crossing underneath tracks of railway station," *Chinese Journal of Underground Space and Engineering*, vol. 9, no. 06, pp. 1412–1418, 2013.
[5] Q. Qu and H. R. Yu, "Construction risk analysis and countermeasure research for shield tunnel passing beneath surface route of urban metro," *Railway Standard Design*, vol. 6, pp. 88–91, 2013, (in Chinese).
[6] Y. F. Wu, "Design plan for frame bridge with multiple lanes and big height difference under existing railway," *China Railway*, vol. 9, pp. 79–82, 2017.
[7] X. Z. Cheng, "Sub-grade reinforcement and rail surface control of shield tunneling under high speed railways," *Urban Mass Transit*, vol. 16, no. 2, pp. 89–94, 2013.
[8] C. Y. Liu, B. L. Wang, and S. H. Zhou, "Shield Tunneling under Railway Station Throats in Soft Areas: A Case Study," *Advances in Civil Engineering*, p. 2020, 2020.
[9] J. S. Huo, B. L. Wang, and S. H. Zhou, "Safety analysis of foundation reinforcement scheme for shield tunnel underpassing intercity railway," *China Railway Science*, vol. 32, no. 5, 2011.
[10] Y. F. Cai, *Research on the Settlement of High-Speed Railway Subgrade Induced by Railway Tunnel Construction Underpassing and Train Vibration," Master Thesis*, Southwest Jiao tong University, Chengdu, China, 2010.
[11] Y. C. Zheng, K. Liu, C. J. Luo, W. G. Qiu, and L. Gong, "Study on simplified calculation model of dynamic train load effect on the lower tunnel," *China Civil Engineering Journal*, vol. 50, no. S1, pp. 25–29, 2017.
[12] S. Samata, H. Ohuchi, and T. Matsuda, "A study of the damage of subway structures during the 1995 Hanshin-Awaji earthquake," *Cement and Concrete Composites*, vol. 19, no. 3, pp. 223–239, 1997.
[13] W. L. Wang, Z. J. Su, J. H. Lin, J. R. Cheng, T. D. Wang, and C. H. Wang, "Discussion on damaged extent of mountainous tunnels due to earthquake, Taiwan," *Modern Tunnelling Technology*, vol. 38, no. 2, pp. 52–60, 2001.
[14] G. C. Wang, J. Yao, L. Sha, L. C. Yu, and X. W. Zheng, "Analysis on the Seismic Response of Hangzhou Metro Tunnel in Soft Soils," *Advanced Materials Research*, vol. 446, pp. 966–969, 2012.
[15] U. Cilingir and S. G. Madabhushi, "Effect of depth on the Seismic response of square tunnels," *Soils and Foundations*, vol. 51, no. 3, pp. 449–457, 2011.
[16] F. Gao and B. S. Guan, *Analysis of Seismic Responses of Shenzhen Subway*, vol. 36, no. 4, pp. 355–359.
[17] China Railway Engineering Design Consulting Group Co., Ltd, "Code for Design on Reinforced and Prestressed Concrete Structure of Railway Bridge and Culvert (TB10002.3-2005, J462-2005)," China Railway Press, Beijing, China, 2005..
[18] S. Sharma and W. R. Judd, "Underground opening damage from earthquakes," *Engineering Geology*, vol. 30, no. 3-4, pp. 263–276, 1991.
[19] Y. M. A. Hashash, J. J. Hook, B. Schmidt, and J. I-Chiang Yao, "Seismic design and analysis of underground structures," *Tunnelling and Underground Space Technology*, vol. 16, no. 4, pp. 247–293, 2001.
[20] V. A. Kontogianni and S. C. Stiros, "Earthquakes and seismic faulting: effects on tunnels," *Turkish Journal of Earth Sciences*, vol. 12, pp. 153–156, 2003.